Phase diagram of a model for ^{3}He-^{4}He mixtures in three dimensions

A. Maciołek,[1] M. Krech,[2,3] and S. Dietrich[2,3]
[1]*Institute of Physical Chemistry, Polish Academy of Sciences, Department III, Kasprzaka 44/52, PL-01-224 Warsaw, Poland*
[2]*Max-Planck-Institut für Metallforschung, Heisenbergstrasse 3, D-70569 Stuttgart, Germany*
[3]*Institut für Theoretische und Angewandte Physik, Universität Stuttgart, Pfaffenwaldring 57, D-70569 Stuttgart, Germany*
(Received 15 April 2003; published 30 March 2004)

A lattice model of ^{3}He-^{4}He mixtures which takes into account the continuous rotational symmetry O(2) of the superfluid degrees of freedom of ^{4}He is studied in the molecular-field approximation and by Monte Carlo simulations in three dimensions. In contrast to its two-dimensional version, for reasonable values of the interaction parameters the resulting phase diagram resembles that observed experimentally for ^{3}He-^{4}He mixtures, for which phase separation occurs as a consequence of the superfluid transition. The corresponding continuum Ginzburg-Landau model with two order parameters describing ^{3}He-^{4}He mixtures near tricriticality is derived from the considered lattice model. All coupling constants appearing in the continuum model are explicitly expressed in terms of the mean concentration of ^{4}He, the temperature, and the microscopic interaction parameters characterizing the lattice system.

DOI: 10.1103/PhysRevE.69.036117 PACS number(s): 05.50.+q, 64.60.Cn, 64.60.Kw, 67.40.Kh

I. INTRODUCTION

Spatial confinements of systems undergoing continuous phase transitions perturb the fluctuation spectrum of the corresponding ordering degrees of freedom. This leads to a dependence of the free energy of the systems on the distance between the confining walls which can be expressed in terms of universal scaling function. Their gradient renders the so-called critical Casimir forces which are the analogs of the well known electromagnetic Casimir or dispersion forces.

Recent developments in the theory of Casimir forces in critical and correlated fluids [1] have provided a strong motivation for testing them experimentally in various systems. Capacity studies of ^{4}He wetting films near the superfluid transition T_λ [2] have confirmed the existence of the critical Casimir effect and for temperatures $T>T_\lambda$ quantitative agreement with corresponding theoretical predictions has been found [3–5]. Similar effects have been observed for wetting films of binary liquid mixtures near the critical end point of their demixing transition [6]. Additional evidence for the critical Casimir force and detailed data have been reported for wetting films at solid substrates of ^{3}He-^{4}He mixtures near their tricritical point [7,8]. These latter experiments have also raised new interesting challenges for the theory, which have motivated the present work. Among them is the sign and the amplitude of the Casimir force or, more generally, the form of its scaling function for different values of the concentration of ^{3}He atoms. Theory predicts that these features of the Casimir force crucially depend on the type of boundary conditions which the confining surfaces impose on the order parameter [1]. For example, the force should be attractive for symmetric boundary conditions and repulsive for nonsymmetric boundary conditions. The distinction between the surface universality classes is also relevant. In the case of pure ^{4}He films near the λ point the boundary conditions at the two confining interfaces of the wetting layer seem to be very well approximated by symmetric Dirichlet boundary conditions forming the so-called ordinary surface universality class, because the quantum-mechanical wave function that describes the superfluid state vanishes at both interfaces [1,2]. For films of ^{3}He-^{4}He mixture the situation is less clear. In these systems a ^{4}He-rich layer forms near the substrate-fluid interface, which may become superfluid already above the λ line [9–11], whereas there is an enrichment of ^{3}He near the opposing fluid-vapor interface. Thus the two interfaces impose a nontrivial concentration profile, which in turn couples to the superfluid order parameter. The experiment of Ref. [7] reports a repulsive Casimir force at the tricritical point, but it is not immediately obvious that the concentration profile induces effectively nonsymmetric boundary conditions for the superfluid order parameter, i.e., symmetry-breaking boundary conditions at the substrate-fluid interface (also known as the so-called extraordinary or normal universality class) and Dirichlet boundary conditions at the fluid-vapor interface. The superfluid order parameter possesses a continuous O(2) symmetry so that if the layer is effectively two dimensional it is in the Kosterlitz-Thouless phase with the superfluid order parameter equal to zero [12]. On the other hand, upon approaching the λ line from the high-temperature side the superfluid layer thickens due to the increase of the correlation length and a dimensional crossover to a three-dimensional superfluid phase with nonzero order parameter should take place [13]. In order to be able to interpret and to understand the features of the Casimir force and other surface and finite-size effects in ^{3}He-^{4}He mixture films near the tricritical point systematic studies of a model system are needed. Due to the universal character of the critical Casimir force it is sufficient to choose as a model system one which belongs to the same universality class as the actual physical system. The prerequisite of such future studies is a detailed analysis of the bulk properties of such a suitable model. This is the purpose of the present paper. The model should resemble the main features of the bulk phase diagram of ^{3}He-^{4}He mixtures in three dimensions ($d=3$) and take into account the continuous rotational O(2) symmetry of the superfluid degrees of freedom of ^{4}He.

The general features of phase separation and superfluidity in three-dimensional mixtures of liquid ^{3}He and ^{4}He are

 ©2004 The American Physical Society

well known from experiments [14]. In pure ^{4}He there is a transition from a normal fluid to a superfluid phase characterized by a complex order parameter. If ^{4}He is diluted with ^{3}He, the superfluid transition temperature is depressed. Simultaneously, the tendency toward phase separation increases and at a critical ^{3}He concentration the mixture undergoes a first-order phase transition into a ^{4}He-rich and a ^{3}He-rich phase, of which only the ^{4}He-rich phase is superfluid. In the temperature-^{3}He concentration plane (T,x) the line of second-order superfluid transitions $T_s(x)$ meets the boundary of the two-phase coexistence region at the tricritical point ($T_t \approx 87$ mK, $x_t \approx 0.67$); $x = N_3/(N_3+N_4)$, where N_i, $i=3$, 4, denotes the number of atoms of ^{3}He or ^{4}He, respectively.

In this paper we consider a simple lattice model known in the literature as the vectoralized Blume-Emery-Griffiths(VBEG) model [15,16]. It is defined in Sec. II. The bulk phase diagram of the VBEG model was investigated only in spatial dimensions $d=2$ by means of Migdal-Kadanoff recursion relations [15,16]; no tricritical point was found for any value of the model parameters. Here we study the three-dimensional version of this model within the molecular-field approximation and by Monte Carlo simulations, and we demonstrate that for reasonable values of interaction parameters the resulting phase diagram resembles topologically that observed experimentally for three-dimensional mixtures, for which the phase separation appears as a consequence of the superfluid ordering. This is carried out in Sec. III and Sec. IV, respectively. In Sec. VI we derive a two-parameter continuous Landau-Ginzburg (LG) model describing bulk ^{3}He-^{4}He mixtures near a tricritical point starting from the modified VBEG model. The LG approach has many advantages and it is worthwhile to have a LG model with coupling constants explicitly related to the measured quantities, such as temperature, superfluid density, concentration of ^{3}He atoms, or parameters describing interactions. We close our paper with a summary and conclusions.

II. THE MODEL

We consider a simple lattice model of ^{3}He-^{4}He mixtures which takes into account the continuous rotational O(2) symmetry of the superfluid degrees of freedom of ^{4}He. It is a vectorial generalization of the spin-1 model used by Blume, Emery, and Griffiths (BEG) [17] for describing the λ line and the tricritical point in ^{3}He-^{4}He mixtures. This description does not aim at a quantitatively faithful modeling of the actual experimental phase diagram [14]. Instead we strive for capturing its essential physical and topological features, i.e., the phase segregation in conjunction with the formation of a superfluid phase. *Inter alia*, this means that the model described in the following does not capture the finite miscibility of ^{3}He in ^{4}He of about 6% at very low temperatures, where the ^{3}He in solution behaves as a Fermi liquid and thus would require a fully quantum-mechanical treatment [18]. This latter aspect has, however, no important physical implications for the phase behavior near the elevated tricritical temperature which is the focus of the present paper.

In this model each simple cubic lattice site i is associated with an occupation variable t_i, taking the values 0 or 1, and a phase θ_i ($0 \leqslant \theta_i < 2\pi$) which mimics the phase of the ^{4}He wave function. A ^{3}He atom at site i corresponds to $t_i=0$ and a ^{4}He atom to $t_i=1$. Since the model in this reduced version does not allow for unoccupied sites, the model does not exhibit a vapor phase. (In future studies the model can be generalized to incorporate the vapor phase; here it is left out for reasons of simplicity.) θ_i reflects the superfluid degrees of freedom. The model Hamiltonian consists of a lattice gas part describing a binary mixture and a term responsible for the "superfluid" ordering. Since only ^{4}He atoms couple to the superfluid order parameter the Hamiltonian is taken as

$$\mathcal{H} = -J\sum_{\langle ij\rangle} t_i t_j \cos(\theta_i - \theta_j) - K\sum_{\langle ij\rangle} t_i t_j + \Delta\sum_i t_i, \quad (1)$$

where the first two sums are over nearest-neighbor pairs $\langle ij\rangle$, and the last sum is over all lattice sites. The lattice constant a is taken to be equal to 1.

In the lattice gas model of the ^{3}He-^{4}He binary mixture the coupling constant K and the field Δ are related to the effective $^\alpha$He-$^\beta$He interactions $-K_{\alpha\beta}$ [19],

$$K = K_{33} + K_{44} - 2K_{34}, \quad (2)$$

and to the chemical potentials μ_3 and μ_4 of ^{3}He and ^{4}He, respectively,

$$\Delta = \mu_3 - \mu_4 + 2z(K_{33} - K_{34}), \quad (3)$$

where z is the coordination number of the lattice ($z=2d$, where d is the spatial dimension of the system; $z=6$ in the present case).

In the liquid the effective interactions $K_{\alpha\beta}$ are different for different α and β due to the differences of mass and statistics between ^{3}He and ^{4}He atoms. The coupling constant J is related [16,22] to a bare, superfluid density $\rho_0(T)$ by

$$J = \hbar^2 \rho_0(T) a^{(d-2)}/m^2, \quad (4)$$

where m is the mass of a ^{4}He atom. a is the mean interparticle spacing (the lattice parameter in the lattice model). The superfluid density can be measured from the velocity of third sound and from the response of a torsional oscillator [20]; it has units of mass per unit volume (or area in two dimensions). Here we are concerned only with the case $J>0$ and $K>0$.

When all occupation numbers t_i are equal to 1, up to constants the first term in Eq. (1) corresponds to the classical XY model (the planar rotator model) for pure ^{4}He. Therefore, in the limit of $\Delta \to -\infty$ the partition function of the model reduces to that of XY model up to a factor e^{KzN} where N is the number of lattice sites.

The model as defined above is known in the literature as the VBEG model. It was first proposed by Berker and Nelson [16] and, independently, by Cardy and Scalpino [15] to describe thin *films* of ^{3}He-^{4}He mixtures, for which the mechanism of the superfluid transition is different from that in $d=3$; there is no spontaneous breaking of the continuous

symmetry in $d=2$ [21], i.e., the order parameter does not become nonzero below the transition temperature. The superfluid transition in films of ^{3}He-^{4}He mixtures is of the Kosterlitz-Thouless type [12].

In $d=2$ the phase diagram of the VBEG model was obtained by means of the Migdal-Kadanoff renormalization-group method [15,16]. Its features are qualitatively similar to those observed experimentally for the corresponding three-dimensional mixtures, except that there is no true tricritical point for any value of the model parameters. The line of the superfluid transitions (λ line) is connected to the phase-separation curve by a critical end point at a temperature distinctly lower than the phase-separation critical temperature. Thus upon lowering the temperature the system first phase separates into two normal fluids with different concentrations of ^{3}He. At lower temperatures, there is phase separation into a superfluid phase with a low ^{3}He concentration and into a normal fluid with a high ^{3}He concentration.

In this paper we are interested in the corresponding three-dimensional systems. We determine the phase diagram of the VBEG model within mean-field approximation and by Monte Carlo simulations.

III. MOLECULAR-FIELD APPROXIMATION

A. Free energy

In this section we determine the phase diagram of the VBEG model within the molecular-field approximation. It is derived from the variational method based upon approximating the total equilibrium density matrix by a product of local site density matrices ρ_i [22].

The variation theorem for the free energy reads

$$F \leqslant F_\rho = \mathrm{Tr}(\rho\mathcal{H}) + (1/\beta)\mathrm{Tr}(\rho \ln \rho), \tag{5}$$

where F is the exact free energy and F_ρ is an approximate free energy associated with the density matrix ρ; $\beta = 1/k_B T$. The minimum of F_ρ with respect to the variation of ρ subject to the constraint $\mathrm{Tr}\rho = 1$ is attained for the equilibrium density matrix, $\rho = e^{-\beta\mathcal{H}}/\mathrm{Tr}(e^{-\beta\mathcal{H}})$.

Within mean-field theory the density matrix is approximated by

$$\rho = \rho_0 = \prod_{i=1}^{N} \rho_i, \tag{6}$$

where in homogeneous bulk systems the local density matrix ρ_i is independent of the site i. For the Hamiltonian given by Eq. (1) the variational mean-field free energy per site is

$$\frac{F_{\rho_0}}{N} \equiv \frac{\Phi}{N} = -\frac{\tilde{K}}{2}[\mathrm{Tr}(t_i\rho_i)]^2 - \frac{\tilde{J}}{2}\{[\mathrm{Tr}(t_i \cos\theta_i \rho_i)]^2 + [\mathrm{Tr}(t_i \sin\theta_i \rho_i)]^2\} + \Delta\,\mathrm{Tr}(t_i\rho_i) + (1/\beta)\mathrm{Tr}(\rho_i \ln \rho_i), \tag{7}$$

where $\tilde{K} = zK$ and $\tilde{J} = zJ$. To determine variational minima to Eq. (7) we treat the local site density ρ_i as a variational function, and the best functional form in terms of t_i and θ_i is obtain by minimizing F_{ρ_0} with respect to ρ_i. In this procedure, however, the connection between F_{ρ_0} and the Hemholtz free energy functional of the order parameters is not straightforward [23]. Minimizing $\Phi/N + \eta\mathrm{Tr}(\rho_i)$ with respect to ρ_i and with η as a Lagrange multiplier, one obtains

$$\rho_i = e^{-\beta h_i}/\mathrm{Tr}(e^{-\beta h_i}), \tag{8}$$

where h_i is the single-site molecular Hamiltonian given by

$$h_i = -\tilde{K}[\mathrm{Tr}(t_i\rho_i)]t_i - \tilde{J}\{[\mathrm{Tr}(t_i \cos\theta_i)]t_i \cos\theta_i + [\mathrm{Tr}(t_i \sin\theta_i)]t_i \sin\theta_i\} + \Delta t_i. \tag{9}$$

We define the following order parameters:

$$Q \equiv 1 - x = \langle t_i \rangle \tag{10}$$

and

$$M_x = \langle t_i \cos\theta_i \rangle, \quad M_y = \langle t_i \sin\theta_i \rangle. \tag{11}$$

Q corresponds to the concentration of ^{4}He, x to the concentration of ^{3}He, and M_x, M_y are the components of the two-dimensional superfluid order parameter $\mathbf{M} = (M_1, M_2)$ with $M = \sqrt{M_x^2 + M_y^2}$. Within this approximation $Q(\Delta, T)$ and $M(\Delta, T)$ are given by two coupled self-consistent equations:

$$Q = \frac{I_0(\beta\tilde{J}M)}{e^{\beta(-\tilde{K}Q+\Delta)} + I_0(\beta\tilde{J}M)} \tag{12}$$

and

$$M = \frac{I_1(\beta\tilde{J}M)}{e^{\beta(-\tilde{K}Q+\Delta)} + I_0(\beta\tilde{J}M)}, \tag{13}$$

where $I_0(z)$ and $I_1(z)$ are modified Bessel functions [24].

The equilibrium free energy $\Phi(\Delta, T)$ is given by

$$\Phi(\Delta,T)/N = \frac{\tilde{K}}{2}[(Q(\Delta,T)]^2 + \frac{\tilde{J}}{2}[M(\Delta,T)]^2 + (1/\beta) \times \ln[1 - Q(\Delta,T)]. \tag{14}$$

Most parts of the phase diagram can only be determined by solving the equations for Q and M numerically. Some regions, however, can be studied analytically.

B. λ line and tricritical point

In order to find the line of critical points on which second-order transitions from the normal ($M=0$) to the the superfluid ($M \neq 0$) state take place, one needs the thermodynamic potential in terms of the order parameter M,

$$A(M, \Delta, T) = \Phi - MH, \tag{15}$$

where H is a field conjugate to M,

$$H = -\frac{\partial A}{\partial M}. \tag{16}$$

The conditions for the critical points are

$$\frac{\partial H}{\partial M}=\frac{\partial^2 H}{\partial M^2}=0, \quad \frac{\partial^3 H}{\partial M^3}>0, \tag{17}$$

and the tricritical point is determined by

$$\frac{\partial H}{\partial M}=\frac{\partial^2 H}{\partial M^2}=\frac{\partial^3 H}{\partial M^3}=\frac{\partial^4 H}{\partial M^4}=0, \quad \frac{\partial^5 H}{\partial M^5}>0. \tag{18}$$

To find H as a function of M we use the analog of Eq. (13) for $H\neq 0$,

$$M=\frac{I_1(\beta\tilde{J}M+\beta H)}{e^{\beta(-\tilde{K}Q+\Delta)}+I_0(\beta\tilde{J}M+\beta H)}. \tag{19}$$

Since this equation cannot be inverted explicitly, we expand it around $H=0$ keeping only terms linear in H, and find

$$\beta H=\frac{I_1(\beta\tilde{J}M)-MI_0(\beta\tilde{J}M)+Me^{\beta(-\tilde{K}Q+\Delta)}}{MI_1(\beta\tilde{J}M)-(1/2)[I_0(\beta\tilde{J}M)-I_2(\beta\tilde{J}M)]}. \tag{20}$$

Applying the conditions formulated in Eqs. (17)–(20) yields the whole line of critical points, i.e., the λ line

$$T_s(x)=\frac{\tilde{J}(1-x)}{2}=\frac{\tilde{J}Q}{2}. \tag{21}$$

It follows that, as the concentration of ^{3}He increases from zero, T_s decreases linearly from $T_s(0)=\tilde{J}/2$. The critical curve $\Delta=\Delta_s(T)$ in the (Δ,T) plane can be obtained by first solving Eq. (12) for Δ (here and in the following we include k_B into T), which gives

$$\Delta(Q,T)=T\ln(1-Q)-T\ln Q+\tilde{K}Q+T\ln I_0(\beta\tilde{J}M), \tag{22}$$

and then evaluate Eq. (22) for $M=0$ and $Q=2T/\tilde{J}$ [see Eqs. (10) and (21)].

The line of second-order phase transitions ends at the tricritical point (T_t,x_t), where the transition changes to a first-order one. From Eqs. (18) and (20) one obtains for the temperature T_t,

$$T_t/T_s(0)=\frac{1+2K/J}{2+2K/J} \tag{23}$$

and for the concentration x_t,

$$T_t/T_s(0)=1-x_t, \tag{24}$$

provided $\partial^5 H/\partial M^5>0$ holds for the chosen value of K/J. It is possible that not all critical points on this so-called critical line represent equilibrium phase transitions because the latter ones are preempted by first-order demixing transitions. Thus it can be that only a portion of this so-called critical line gives the λ line, the rest being metastable.

C. Demixing

For the disordered phase with $M=0$ one can easily find the first-order phase-separation line from the ^{3}He-rich ''normal'' fluid to the ^{4}He-rich ''normal'' fluid. The phase separation is associated with an instability loop including a range of Q values for which $\partial\Delta/\partial Q>0$ and the critical point is given by $\partial\Delta/\partial Q=\partial^2\Delta/\partial Q^2=0$. These last two relations together with Eq. (22), evaluated at $M=0$, are satisfied if $Q_c=1/2$ and $T_c=\tilde{K}/4$. The critical value Δ_c of Δ is $\tilde{K}/2$. Inserting $\Delta=\Delta_c$ and $M=0$ into Eq. (22) gives

$$T\ln\frac{1-Q}{Q}-(1/2)\tilde{K}(2Q-1)=0. \tag{25}$$

For $T<\tilde{K}/4$ this equation has pairs of solution $(Q,1-Q)$. For $M=0$, i.e., above the critical line in the (Q,T) plane, these solution form the coexistence curve which is symmetric about $Q=1/2$ or $x=0.5$. For temperatures lower than the intersection temperature T_I of the critical line with the curve given by Eq. (25), the phase rich in ^{4}He becomes superfluid and Eq. (25) no longer represents the coexistence curve.

In order to find what types of phase diagrams the present model provides we look for the phase-separation instability on the critical curve as determined in Sec. III B and how it is located with respect to the intersection point $P_I=(Q_I,T_I)$. Depending on the ratio K/J there are three possibilities which give three different types of the phase diagram: (i) the instability point P_t lies below the intersection point P_I, (ii) P_t lies above P_I, and (iii) the critical point of the transition between ^{3}He- and ^{4}He-rich ''normal'' fluids falls into the instability range initiated at P_t.

A sufficient condition for an instability loop leading to phase separation is $\partial\Delta/\partial Q>0$. Using Eq. (22) and the relation $Q=MI_0(\beta\tilde{J}M)/I_1(\beta\tilde{J}M)$, one finds

$$\left(\frac{\partial\Delta}{\partial Q}\right)_{Q=Q^{*}+}=\frac{-\tilde{J}}{2(1-Q^{*})}+\tilde{K}+\tilde{J}, \tag{26}$$

whereas

$$\left(\frac{\partial\Delta}{\partial Q}\right)_{Q=Q^{*}-}=\frac{-\tilde{J}}{2(1-Q^{*})}+\tilde{K}, \tag{27}$$

where Q^{*} is the critical value of Q for superfluid ordering given by Eq. (21). Thus $(\partial\Delta/\partial Q)_{Q=Q^{*}-}>(\partial\Delta/\partial Q)_{Q=Q^{*}+}$ and the instability will occur on the ordered side of the critical curve when $(\partial\Delta/\partial Q)_{Q=Q^{*}+}=0$. From Eq. (26) the coordinates of the instability point P_t are given by Eq. (23), i.e., they are exactly the same as those of the tricritical point. We find numerically that P_I and $P_t=(Q_t,T_t)$ coincide for $K/J\approx 2.016\,81$.

For $K/J>2.016\,81$ case (i) is realized, i.e., the instability point P_t lies inside the coexistence curve between the ^{3}He-rich normal fluid and the ^{4}He-rich normal fluid. We have obtained numerically the phase diagram for $K/J=2.4$. It is shown in Figs. 1(a) and 1(b) in the (Δ,T) and (x,T) planes, respectively. The solid line in the (Δ,T) plane repre-

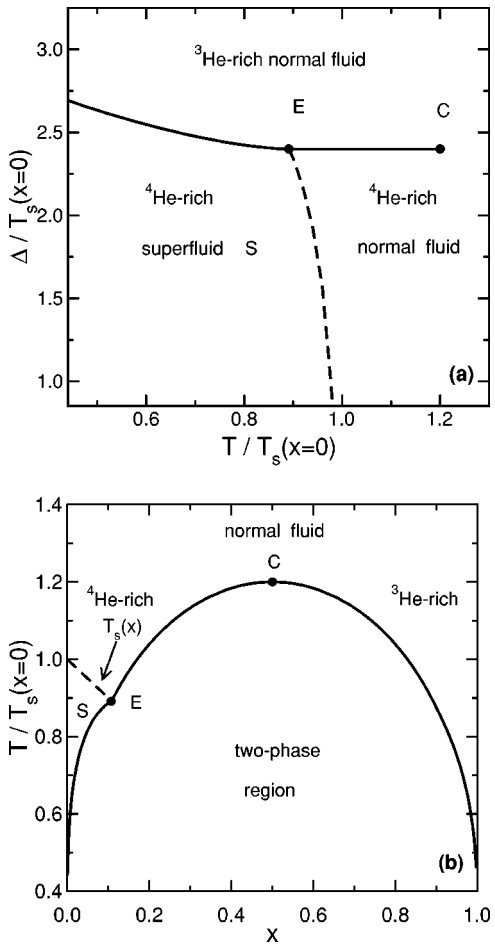

FIG. 1. Phase diagram in the (Δ,T) (a) and (x,T) (b) planes for the model given by Eq. (1) obtained within mean-field theory for $K/J=2.4$. Δ and T are measured in units of the critical temperature $T_s(0)$ of XY model on a simple cubic(s.c.) lattice in $d=3$ for $J=K$. x (dimensionless) is the ^{3}He concentration. There are three phases which can be identified as a ^{3}He-rich normal fluid ($M=0$, $x=1-Q$ large), a ^{4}He-rich normal fluid ($M=0$, x small), and a ^{4}He-rich superfluid S ($M\neq 0$, x small). In (a) the dashed line represents second-order phase transitions and corresponds to the λ line; full lines are the loci of first-order phase transitions. For this value of K/J there is no tricritical point. The λ line of second-order phase transitions terminates at the phase-separation curve at the critical end point E. The two-phase region in (b) and the line of first-order phase transitions in (a) end at a critical point C. The coordinates of the critical points are $C=[\Delta/T_s(0)=2.4, T/T_s(0)=1.2]$, $E=[\Delta/T_s(0)=2.4, T/T_s(0)\approx 0.89]$ and $C=[T/T_s(0)=1.2, x=1/2]$ and $E=[T/T_s(0)\approx 0.89, x\approx 0.107]$. In (b) the λ line is given by $T_s(x)/T_s(0)=1-x$ [see Eq. (21)]. The two-phase region in (b) between C and E is symmetric about $x=1/2$.

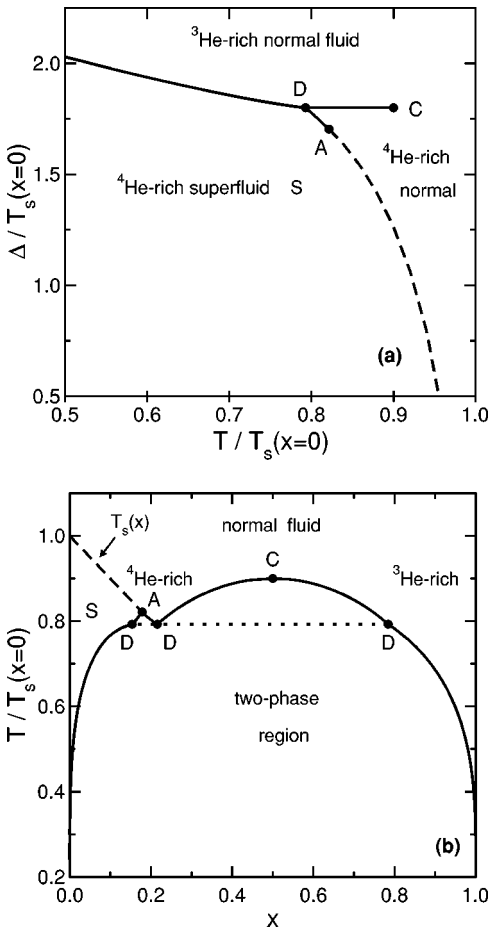

FIG. 2. Same as Fig. 1, but for $K/J=1.8$. For this value of K/J the λ line ends at a tricritical point A beyond which there is a first-order phase transition between the ^{4}He-rich superfluid S and the ^{4}He-rich normal fluid. At even lower temperatures there is a triple point D. The coordinates of these points are $A=[\Delta/T_s(0)\approx 1.704, T/T_s(0)\approx 0.821]$, $C=[\Delta/T_s(0)=1.8, T/T_s(0)=0.9]$, $D=[\Delta/T_s(0)=1.8, T/T_s(0)\approx 0.793]$ and $A=[T/T_s(0)\approx 0.821, x\approx 0.179]$, $C=[T/T_s(0)=0.9, x=1/2]$, $D=[T/T_s(0)=0.793, x_1\approx 0.154, x_2\approx 0.216, x_3\approx 0.784]$. In (b) there are two-phase coexistence regions below A and below C which join for three-phase coexistence at D (dotted curve).

sents the line of equilibrium second-order phase transitions on the critical curve and thus represents the λ line. This line terminates at the phase-separation curve (dashed line) at the *critical end point E*. CE is the line of the first-order phase transitions between the ^{3}He-rich and the ^{4}He-rich normal fluids with the critical point C. At the point E the curve CE turns into the line of first-order phase transitions between the ^{3}He-rich normal fluid and the ^{4}He-rich superfluid. The phase boundary $\Delta(T)$ between the ^{3}He-rich and the ^{4}He-rich normal fluid or the ^{4}He-rich superfluid (represented by a dashed line) is expected to exhibit a singular curvature $\sim|T-T_E|^{-\alpha}$ as T approaches the end point temperature from above or below [25]. α is the critical exponent describing the specific heat singularity on the critical line below the point E. Since in mean-field theory $\alpha=0$, there is no nonanalyticity at the end point within the present approach. In the (x,T) plane [see Fig. 1(b)] the coexistence curve is smooth at $T=T_E$ on the ^{3}He-rich side.

For $K/J<2.016\,81$ the instability point P_t lies outside the coexistence curve for the ^{3}He-rich normal fluid and the ^{4}He-rich normal fluid. Therefore, as T decreases below T_t, the phase separation between the ^{3}He-rich normal fluid and the ^{4}He-rich superfluid commences at the point P_t on the critical curve; hence $P_t\equiv A$ is a *tricritical point*. The phase diagram for $K/J=1.8$ is shown in Fig. 2. In the (Δ,T) plane

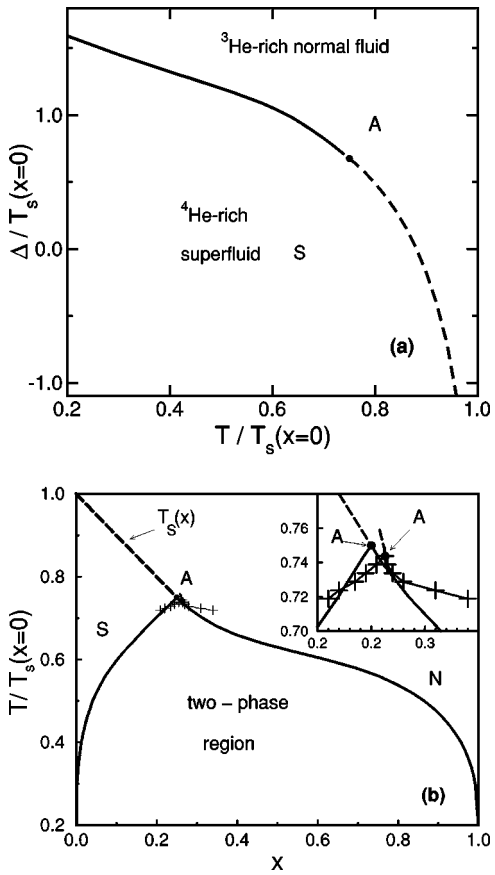

FIG. 3. Same as Figs. 1 and 2, but for $K/J=1$. The λ line $T_s(x)$ and the first-order phase-separation line meet at the tricritical point *A*. The ^{3}He-rich "normal" fluid phase is denoted by *N*. In (b) Monte Carlo data for the phase boundaries are indicated by pluses which are connected by thin lines representing the Monte Carlo phase boundaries. The inset shows the results on an expanded scale near the tricritical point *A*. The coordinates of the tricritical point within mean-field theory are $A=[\Delta/T_s(0)\approx 0.776,\ T/T_s(0)=0.75]$ and $A=[T/T_s(0)=0.75,\ x=0.25]$. In (b) the tricritical point *A*, as obtained from Monte Carlo data, is also denoted by a dot and has the coordinates $[T/T_s(0)=0.744,\ x=0.26]$.

[Fig. 2(a)] the first-order transition line between the ^{3}He-rich normal fluid and the ^{4}He-rich superfluid which starts at *A* terminates at a triple point *D* where it meets the first-order transition lines between the ^{3}He-rich normal fluid and the ^{4}He-rich normal fluid (curve *CD*) and between the ^{3}He-rich normal fluid and the ^{4}He-rich superfluid.

For even smaller value of the ratio K/J there are no longer two distinguishable disordered phases, i.e., the line *DC* in Fig. 2(a) has shrunk to zero. The critical point for coexistence between the ^{3}He-rich normal fluid and the ^{4}He-rich normal fluid, which occurs at $x_c=1/2$ and $T_c=\tilde{K}/4$, disappears. In Fig. 3 we present the phase diagram for $K/J=1$. In the (Δ,T) plane it exhibits a very simple form [Fig. 3(a)]. The λ line meets the first-order transition line between the ^{3}He-rich normal fluid and the ^{4}He-rich superfluid at the *tricritical point A*. The lines meet with a common tangent, a feature characteristic of the mean-field approximation. In the (x,T) plane [Fig. 3(b)] at the tricritical point the critical line $T_s(x)$ has the same slope as the phase-separation curve on the ^{3}He-rich side. The emergence of the type of phase diagram shown in Fig. 3 from the one shown in Fig. 2 takes place at that value of K/J for which there is an equilibrium between the phase at the critical point *C* and an ordered phase yielding $K/J\approx 1.4298$. For K/J slightly less than this value $K/J=1.4298$, the tricritical point is located at $T_t\approx 0.397$ and $x_t\approx 0.206$. Within mean-field theory the ^{3}He-rich side of the coexistence curve has a plateau for $0.8\lesssim x\lesssim 0.3$, i.e., right below the tricritical point small changes in temperature lead to pronounced changes in the concentration of ^{3}He. As K/J is reduced further, the tricritical point shifts to larger values of x and smaller values of T. Also the shape of the coexistence curve changes; the plateau disappears and the concentration of ^{3}He increases more uniformly with the temperature.

A phase diagram like that of Fig. 3 resembles qualitatively the experimental one [14], for which one finds for the tricritical point $T_A/T_s(0)=0.4$ and $x_A=0.669$. In our model x_A is, however, always smaller than 0.5.

IV. MONTE CARLO SIMULATIONS

For the Monte Carlo treatment of the model Hamiltonian given by Eq. (1) a ^{4}He atom is represented by the normalized spin vector

$$\mathbf{S}_i\equiv(\cos\theta_i,\sin\theta_i) \tag{28}$$

for each lattice site *i* in the spirit of the standard *XY* model. A ^{3}He atom on lattice site *i* is represented as $\mathbf{S}_i\equiv(0,0)$. Consequently the occupation number t_i on lattice site *i* is given by $t_i=|\mathbf{S}_i|$ and the interaction $\cos(\theta_i-\theta_j)$ between two ^{4}He atoms is given by the computationally more favorable scalar product $\cos(\theta_i-\theta_j)=\mathbf{S}_i\cdot\mathbf{S}_j$. The lattice is simple cubic with periodic boundary conditions and *L* lattice sites in each direction. The Monte Carlo algorithm is based on various standard procedures which we discuss briefly in the following.

In order to explore the phase space of the model, two types of updates are needed: (i) spin flip updates and (ii) particle insertion and deletion updates. The spin flip updates are responsible for the creation of long-ranged magnetic order which in our model represents the normal-superfluid transition. This can be of first or second order depending on the concentration $x=1-\langle t_i\rangle$ of ^{3}He ($t_i=0$) in the system (see Fig. 3). The particle insertion and deletion updates are responsible for the demixing transition (phase separation) in our model. This transition can also be first or second order depending on the coupling constants in the model (see Figs. 1 and 2). In our simulation we are primarily interested in that regime of coupling constants, for which the phase diagram resembles that of actual ^{3}He-^{4}He mixtures (Fig. 3) and therefore the possibility of a second-order (critical) demixing transition is not taken into account for the selection of the Monte Carlo moves. We therefore use the following methods in our Monte Carlo simulation: (i) single particle insertion and deletion and (ii) single spin flip according to the Metropolis algorithm [26], (iii) single cluster spin flip according to the Wolff algorithm [27], and (iv) overrelaxation updates

of the spin degrees of freedom at constant configurational energy [28]. For each particle insertion or single spin flip move the new spin state is randomly selected from the even distribution on the unit circle. The projection vector for the embedding part of the Wolff algorithm [27] is also chosen randomly from the even distribution on the unit circle.

The above update methods are performed in sweeps over the whole lattice, where *each* spin flip sweep (ii), (iii), or (iv) is preceded by a Metropolis particle insertion and deletion sweep (i). Cluster updates of the particle configuration according to the embedding algorithm of Ref. [27] are disregarded, because the critical demixing transition will not be explored here.

The three basic Monte Carlo updates (ii)–(iv) outlined above are combined according to the hybrid Monte Carlo idea [29] to ensure efficient configuration space exploration also for second-order (critical) transitions to long-ranged magnetic order. One hybrid Monte Carlo step consists of ten individual steps, each of which can be one of the updates listed above. The Metropolis and the Wolff algorithm work the standard way, in which the acceptance probability p of a proposed spin flip in the Metropolis algorithm is defined by the local heat bath rule

$$p(\Delta E) = 1/[\exp(\Delta E/k_B T) + 1], \tag{29}$$

where ΔE is the change in configurational energy of the proposed move. The overrelaxation part of the algorithm performs a microcanonical update of the configuration by sequentially reflecting each spin in the lattice at the direction of the local field, i.e., the sum of the nearest-neighbor spins, such that its contribution to the energy of the whole configuration remains constant. The implementation of this update scheme is straightforward, because according to Eq. (1) the energy of a spin with respect to its neighborhood has the functional form of a scalar product. The form hybrid Monte Carlo step depends on the region of the phase-diagram to be explored. In the vicinity of the first-order phase separation line typically six Metropolis (M), one single cluster Wolff (C), and three overrelaxation (O) updates are performed. The individual updates are mixed automatically in the program to generate the update sequence $M\,M\,O\,M\,O\,M\,M\,O\,M\,C$ for the magnetic degrees of freedom.

The random number generator is the shift register generator R1279 defined by the recursion relation $X_n = X_{n-p} \oplus X_{n-q}$ for $(p,q) = (1279,1063)$. Generators like these are known to cause systematic errors in combination with the Wolff algorithm [30]. However, for lags (p,q) used here these errors are far smaller than typical statistical errors. They are further reduced by the hybrid nature of the algorithm [29].

The hybrid algorithm is well suited to explore second-order phase transitions. However, it is unable to overcome the exponential slowing down of the algorithms included in our hybrid scheme in the vicinity of a first-order transition, e.g., the first-order magnetic (i.e., superfluid) transition for higher concentrations of ^{3}He particles, i.e., for occupation numbers $t_i = 0$ in our model. In order to resolve this problem while keeping the benefits of the hybrid scheme we have embedded the hybrid Monte Carlo method in a simulated tempering environment [31]. According to the simulated tempering idea the temperature is treated as a random variable which performs a random walk inside a predefined temperature interval. In our simulation this temperature interval is represented by a discrete set of temperatures, which are spaced closely enough to allow sufficient overlap of the corresponding energy distribution functions. The required reweighting factors [31] are estimated from short runs, one for each pair of neighboring temperatures, and checked *a posteriori* by monitoring the probability distribution of the temperatures—which should be essentially flat—during the production run. Deviations of up to 20% from a flat temperature distribution are tolerated.

The Monte Carlo scheme described above is employed for lattice sizes L between $L = 12$ and $L = 60$. For each choice of parameters we have performed at least 12 blocks of 10^3 hybrid steps for equilibration followed by another 10^3 hybrid steps to estimate the reweighting factors for each pair of neighboring temperatures and finally followed by 4×10^4 hybrid steps for measurements. The measurement block is controlled by an outer loop in which a new temperature is proposed according to the predetermined weight factors [31] after each hybrid Monte Carlo step. Apart from standard thermodynamic quantities the distribution functions of the total energy, the density, and the modulus of the magnetization are monitored using histogram reweighting and extrapolation techniques [32] within the measurement block. Their statistical errors are estimated following standard procedures resulting from the statistical independence of different measurement blocks. Unless otherwise stated, all error bars quoted in the following correspond to one standard deviation. They are displayed only when they exceed the symbol sizes. The simulations have been performed on DEC Alpha Workstations and Pentium III PCs.

V. MONTE CARLO RESULTS

Our primary interest in this study is to use Eq. (1) to model ^{3}He-^{4}He mixtures in the tricritical region and we therefore restrict the numerical investigation of the statistical model described by Eq. (1) to the case $J = K$ for which the phase diagram corresponding to this model Hamiltonian has the same topology as for the liquid phases of ^{3}He-^{4}He mixtures. The tricritical point marks the onset of demixing into a spin (^{4}He) rich fluid and a vacancy (^{3}He) rich fluid, where the spin rich fluid simultaneously exhibits long-ranged magnetic order of the XY type (superfluidity).

The phase diagram is most conveniently investigated by the inspection of distribution functions (histograms) for various thermodynamic quantities [33]. However, the computational expense of the method described in Ref. [33] in $d = 2$ is prohibitive in $d = 3$ for any appreciable system sizes. We therefore resort to a simpler, though less accurate, approach which allows us to treat larger systems and is accurate enough for our purposes. In the following all temperatures are measured in units of the critical temperature $T_s(0)$ of the XY model on a simple cubic lattice in $d = 3$, which is given by $K_c \equiv J/[k_B T_s(0)] = 0.454\,15(5)$ [34]. The chemical

potential Δ is measured in units of the magnetic coupling constant J [see Eq. (1)].

A. Order parameter distribution at tricriticality

The key feature of the ^{3}He-^{4}He phase diagram is the presence of a tricritical point. The task to locate the tricritical point for the model Hamiltonian given by Eq. (1) is aided by the observation that $d=3$ is the upper critical dimension for tricriticality. It is therefore reasonable to assume that the distribution function of the magnetic order parameter essentially takes the mean-field (Landau) form. We will give some *a posteriori* evidence below that this assumption is indeed correct, but an accurate numerical proof of it is beyond the scope of this paper.

The magnetic order parameter, i.e., the magnetization is defined by

$$\mathbf{M}=(M_x,M_y)\equiv L^{-3}\sum_i t_i\mathbf{S}_i, \tag{30}$$

where $t_i=0,1$ characterizes the presence of ^{3}He or ^{4}He at lattice site i and $\mathbf{S}_i=(\cos\theta_i,\sin\theta_i)$ is the standard spin variable of the XY model. In terms of the modulus $m\equiv|\mathbf{M}|$ of the order parameter the distribution function $P(m)$ is assumed to take the form

$$P(m)=P_0 m\exp(-Am^2-Bm^4-Cm^6) \tag{31}$$

according to Landau theory in the tricritical region, where the absence of symmetry-breaking fields is assumed. The parameters A, B, and C essentially play the role of the Landau-Ginzburg model parameters (see Sec. VI below) and they depend on the temperature T and the chemical potential Δ [see Eq. (1)], where C is manifestly positive, but A and B may change sign. For system sizes $L=12$, 18, 24, 36, 48, and 60 simulations have been performed along various paths in the (T,Δ) plane of the phase diagram and the data recorded for $P(m)$ have been fitted according to Eq. (31) using P_0, A, B, and C as fit parameters. For each system size L a pseudotricritical point $[T_t(L),\Delta_t(L)]$ has been identified by the requirement $A=B=0$ within the corresponding statistical error. It turns out that Eq. (31) indeed captures the shape of $P(m)$ rather accurately over several orders of magnitude for P in the pseudotricritical regime (see below). In particular, higher powers of m compatible with the symmetry such as m^8 can be safely ignored. Possible logarithmic corrections to $P(m)$ [35] could not be identified from the numerical data unambiguously. We will comment on other logarithmic corrections later.

B. The tricritical point

From the procedure outlined above we obtain a sequence of pseudotricritical points $[T_t(L),\Delta_t(L)]$ which can be extrapolated to the bulk limit $L\to\infty$. In order to do this one has to identify the functional form of the L dependence of the pseudotricritical point. Within our mean-field picture of the tricritical behavior of our model the coefficients A and B in Eq. (31) are given by the linear combination

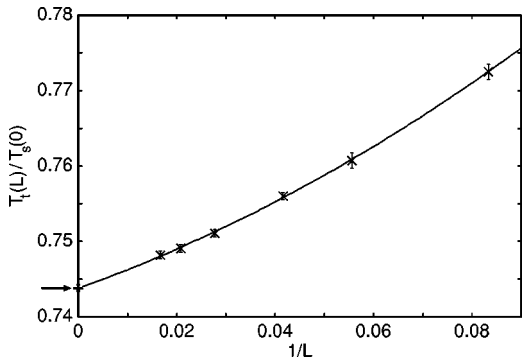

FIG. 4. Pseudotricritical temperature $T_t(L)(\times)$ vs $1/L$ measured in units of the critical temperature $T_s(0)$ of the XY model on a s.c. lattice in $d=3$ for $J=K$ [see Eq. (1)]. L is in units of lattice constant. Error bars correspond to one standard deviation. The solid line shows the fit of Eq. (33) to the numerical data. The arrow indicates the extrapolated value T_t (see main text). The reduced χ^2 of the fit is 0.15.

$$\begin{pmatrix} B \\ A \end{pmatrix} = \mathcal{M}\begin{pmatrix} T-T_t \\ \Delta-\Delta_t \end{pmatrix} \tag{32}$$

in the vicinity of the tricritical point, where $\mathcal{M}$ is the coefficient matrix. From Eq. (32) and finite-size scaling arguments one concludes that for sufficiently large L, $T_t(L)-T_t$ and $\Delta_t(L)-\Delta_t$ are governed by a linear combination of L^{-d_A} and L^{-d_B}, where d_A and d_B are the scaling dimensions of the parameters A and B in Eq. (31) given by $d_A=2$ and $d_B=1$ apart from logarithmic corrections [35]. We therefore arrive at the following functional form of $T_t(L)$ and $\Delta_t(L)$:

$$T_t(L)=T_t+\frac{t_1}{L}+\frac{t_2}{L^2},$$

$$\Delta_t(L)=\Delta_t+\frac{\delta_1}{L}+\frac{\delta_2}{L^2}, \tag{33}$$

where the coefficients t_1, t_2, δ_1, and δ_2 can be obtained from the inverse matrix $\mathcal{M}^{-1}$ and the finite-size relations

$$A=aL^{-2} \quad \text{and} \quad B=bL^{-1} \tag{34}$$

for A and B evaluated at $(T,\Delta)=[T_t(L),\Delta_t(L)]$ for any system size L. The coefficients a and b are nonuniversal metric factors. Equation (33) is used to fit the numerical data for $T_t(L)$ and $\Delta_t(L)$ in order to obtain an estimate for the location of the tricritical point. Logarithmic corrections as given in Ref. [35] can be included in Eq. (33), but they are omitted here because the quality of fit does not change substantially when they are included. The results are shown in Figs. 4 and 5. The finite-size behavior of $T_t(L)$ and $\Delta_t(L)$ is accurately captured by Eq. (33). Both the coefficients t_1, t_2 and δ_1, δ_2 have the same sign and the second coefficient is substantially larger that the first one in both cases. Therefore both coefficients must be kept in order to obtain an acceptable fit. The

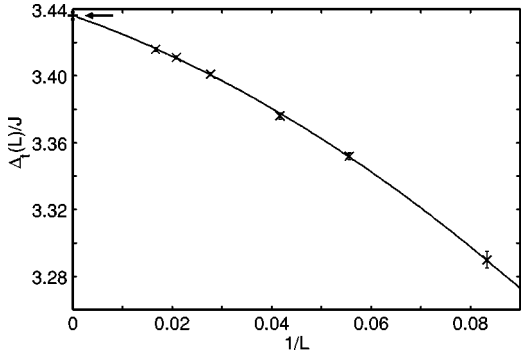

FIG. 5. Pseudotricritical chemical potential $\Delta_t(L)$ ($\times$) vs $1/L$ measured in units of the coupling constant J [see Eq. (1)] for $J=K$. L is in units of lattice constant. Error bars correspond to one standard deviation. The solid line shows the fit of Eq. (33) to the numerical data. The arrow indicates the extrapolated value Δ_t (see main text). The reduced χ^2 of the fit is 0.42.

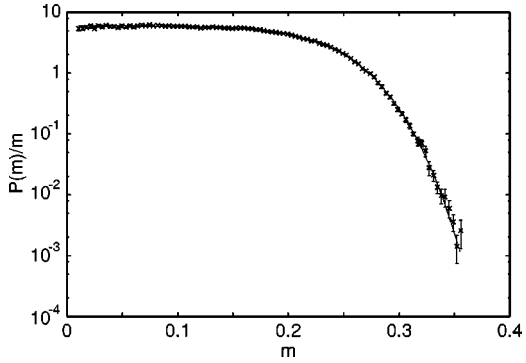

FIG. 6. Least square fit of Eq. (31) (solid line) to the simulation data for $P(m)$ for $L=36$ at $T=T_t(36)$ and $\Delta=\Delta_t(36)$ ($\times$) corresponding to $A=B=0$. All data points except very few are connected by the fit function within their error bars. The reduced χ^2 of the fit is 0.71. $P(m)$ and m are dimensionless.

quality of fit can be measured in terms of the reduced χ^2 which is 0.15 in Fig. 4 and 0.42 in Fig. 5. We thus obtain the extrapolated values

$$T_t/T_s(0)=0.7438(4), \quad \Delta_t/J=3.436(2) \tag{35}$$

as our estimate for the location of the tricritical point, where the statistical uncertainty affects the last digit by the amount given in parentheses. In these units the coefficients in Eq. (33) are given by

$$t_1/T_s(0)=0.23\pm0.02, \;\; t_2/T_s(0)=1.34\pm0.24,$$

$$\delta_1/J=-1.05\pm0.11, \;\; \delta_2/J=-8.5\pm1.4. \tag{36}$$

Another aspect of Eq. (33) is field mixing [33], because the finite-size corrections L^{-1} and L^{-2} are uniquely related to the coefficients (scaling fields) B and A in Eq. (31), respectively. In the vicinity of the tricritical point one therefore obtains from Eqs. (32), (33), and (34) by a matrix inversion

$$\begin{pmatrix} B/b \\ A/a \end{pmatrix} = \frac{1}{t_1\delta_2 - t_2\delta_1} \begin{pmatrix} \delta_2 & -t_2 \\ -\delta_1 & t_1 \end{pmatrix} \begin{pmatrix} T-T_t \\ \Delta-\Delta_t \end{pmatrix}. \tag{37}$$

According to our mean-field picture of tricriticality in $d=3$ the coexistence line $\Delta=\overline{\Delta}(T)$ in the vicinity of $T=T_t$ should be associated with the line $B=\text{const}=0$ in the vicinity of $A=0$. If we linearize the coexistence line near the tricritical point according to

$$\overline{\Delta}(T)=\Delta_t+\Delta_t'(T-T_t) \tag{38}$$

we obtain from Eqs. (36) and (37) for the slope Δ_t' at the tricritical point

$$\Delta_t'=\delta_2/t_2=(6.4\pm2.2)J/T_s(0). \tag{39}$$

Despite its large statistical error this result serves as a valuable guideline for the further exploration of the phase diagram.

The foundation of the above estimates is the quality of the fits of Eq. (31) to the measured order parameter distribution functions. We illustrate the quality of these fits in Fig. 6 for $L=36$ at the corresponding pseudotricritical point $T=T_t(36)$ and $\Delta=\Delta_t(36)$. The shape of the distribution function P is essentially captured by Eq. (31) over more than three orders of magnitude. The parameters A and B vanish within their statistical errors. The reduced χ^2 of the fit is 0.71. If $A=B=0$ is enforced, i.e, the fit is performed only with the parameters P_0 and C, the reduced χ^2 increases to 0.92. For all other system sizes investigated the situation is similar. We will return to the finite size behavior of $P(m)$ after the discussion of finite-size scaling.

C. Finite-size scaling

A naive finite-size scaling ansatz for a thermodynamic quantity $X(A,B,L)$ near a tricritical point in $d=3$ is given by [compare Eq. (31)]

$$X(A,B,L)=L^{-d_X}f_X(AL^2,BL), \tag{40}$$

where $f_X(x,y)$ is the finite-size scaling function associated with the quantity X and d_X is its scaling dimension. Logarithmic corrections have been disregarded for simplicity. For the sequence of the pseudotricritical points $(T,\Delta)=[T_t(L),\Delta_t(L)]$ one has $A=aL^{-2}$ and $B=bL^{-1}$ [see Eq. (34)]. In this case one therefore expects X to display the scaling behavior

$$X(aL^{-2},bL^{-1},L)=L^{-d_X}f_X(a,b)\equiv X_0L^{-d_X}, \tag{41}$$

which can be conveniently checked numerically. However, near tricritical points in $d=3$ one has to consider logarithmic corrections to the naive scaling and these have been examined in Ref. [35]. We therefore only quote the results corresponding to Eq. (41) for the average magnetization $\langle m\rangle$, the specific heat $\mathcal{C}$, and the magnetic susceptibility $\mathcal{X}$. One obtains

$$\langle m\rangle = m_0\left(\frac{L}{l_0}\right)^{-1/2}\left(\ln\frac{L}{l_0}\right)^{1/4},$$

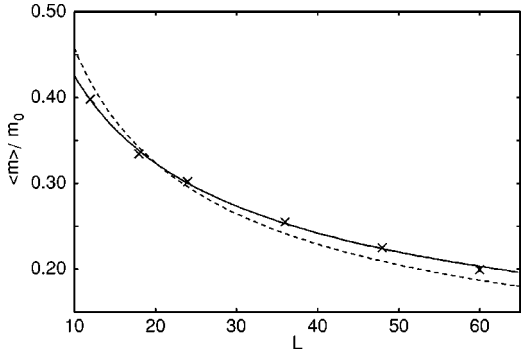

FIG. 7. Least square fit of Eq. (42) (solid line) to the simulation data for $\langle m \rangle$ (dimensionless) ($\times$). A fit to pure mean-field behavior is shown for comparison (dashed line). Data and fit are normalized to the amplitude m_0 and $l_0 = 1.3 \pm 0.3$. For $L = 18$ and $L = 60$ the data points deviate from the fit curve (solid line) by an amount larger than the statistical error. L is in units of lattice constant.

$$\mathcal{C} = \mathcal{C}_0 \frac{L}{l_0} \left(\ln \frac{L}{l_0} \right)^{1/2},$$

$$\mathcal{X} = \mathcal{X}_0 \left(\frac{L}{l_0} \right)^2 \left(\ln \frac{L}{l_0} \right)^{1/4}, \tag{42}$$

where the nonuniversal amplitudes m_0, $\mathcal{C}_0$, $\mathcal{X}_0$ and the length scale l_0 are used as fit parameters. The corresponding results are summarized in Figs. 7–9. The data are compatible with the finite-size scaling behavior given by Eq. (42) (solid lines). The logarithmic corrections turn out to be essential. Disregarding these leads to pure mean-field behavior which is not compatible with the data (dashed lines). For the specific heat displayed in Fig. 8 deviations from the expected behavior occur for larger system sizes $L = 48$ and $L = 60$. These may be due to the proximity to the first-order demixing transition, which is characterized by a finite latent heat. Including a finite background contribution to the specific heat as an additional fit parameter does not improve the fit.

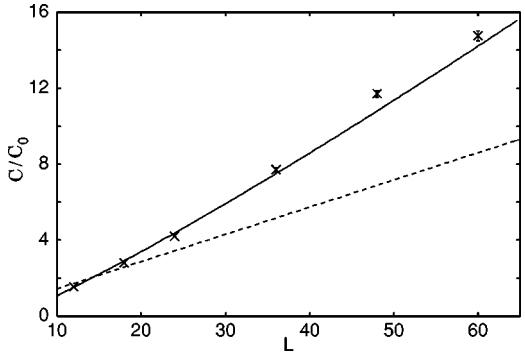

FIG. 8. Least square fit of Eq. (42) (solid line) to the simulation data for the specific heat $\mathcal{C}$ ($\times$). A fit to pure mean-field behavior is shown for comparison (dashed line). Inclusion of a background contribution to $\mathcal{C}$ as an additional fit parameter does not improve the fit. Data and fit are normalized to the amplitude $\mathcal{C}_0$ and $l_0 = 6.3 \pm 0.5$. The deviations from the expected behavior (solid line) for larger systems may be due to the vicinity of the first-order demixing transition. L is in units of lattice constant.

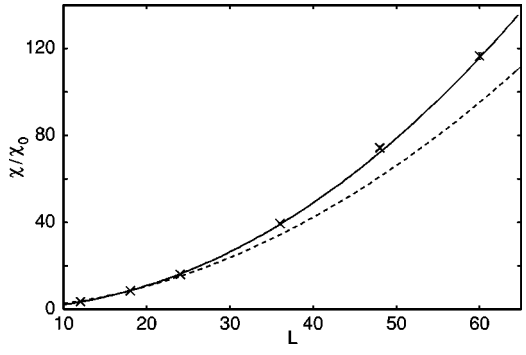

FIG. 9. Least square fit of Eq. (42) (solid line) to the simulation data for magnetic susceptibility $\mathcal{X}$ ($\times$). A fit to pure mean-field behavior is shown for comparison (dashed line). Data and fit are normalized to the amplitude $\mathcal{X}_0$ and $l_0 = 6.2 \pm 0.4$. L is in units of lattice constant.

In particular, the attempt to fit pure mean-field behavior to the data shown in Fig. 8 leads to a negative value for the background specific heat which is inconsistent with thermodynamics. The susceptibility shown in Fig. 9 appears to agree with the expectation for all system sizes whereas the average magnetization shown in Fig. 7 displays a deviation for $L = 60$. The values of l_0 obtained from the fits shown in Figs. 8 and 9 are consistent ($l_0 = 6.3 \pm 0.5$ and $l_0 = 6.2 \pm 0.4$, respectively) whereas $l_0 = 1.3 \pm 0.3$ obtained from $\langle m \rangle$ according to Fig. 7 deviates strongly from the aforementioned estimates for l_0. One of the reasons may be that $\langle m \rangle$ depends rather weakly on L and l_0 as compared to $\mathcal{C}$ and $\mathcal{X}$. Therefore the estimation of l_0 from $\langle m \rangle$ is more susceptible to statistical or systematic errors in the magnetization data. The large relative error of the actual estimate $l_0 = 1.3 \pm 0.3$ seems to indicate this. Corrections to the leading asymptotic behavior given by Eq. (42), which cannot be taken into account on our current data basis, may therefore also play a role.

The scaling behavior of the order parameter distribution function $P(m)$ within the scope of Eq. (31) is determined by the finite-size behavior of the parameter C. In order to compensate the finite-size effects induced by $\langle m \rangle$ we define the effective coupling parameter

$$C_{eff} \equiv C \langle m \rangle^6, \tag{43}$$

where C is taken from the fit of Eq. (31) to the distribution function data along the sequence of the pseudotricritical points ($A = B = 0$) and $\langle m \rangle$ is taken from the fit of Eq. (42) to the magnetization data. The numerical result for C_{eff} according to Eq. (43) is displayed in Fig. 10 which shows a slow but systematic decrease of C_{eff} with the system size. According to the renormalization-group theory of tricritical behavior C_{eff} should play the role of the coupling constant at tricriticality, which is a dangerous irrelevant variable in $d = 3$ [35]. We therefore expect the finite-size behavior [35]

$$C_{eff}(L) = \left(c_0 + c_1 \ln \frac{L}{l_0} \right)^{-1} \tag{44}$$

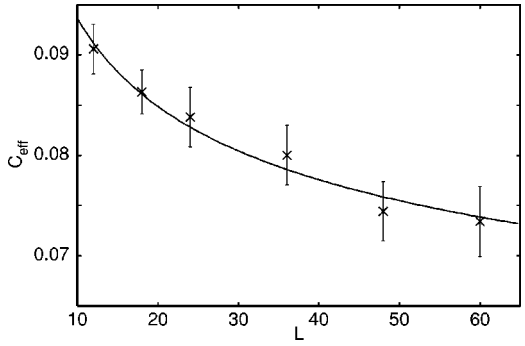

FIG. 10. Effective coupling parameter C_{eff} (dimensionless) according to Eq. (43) ($\times$) and a least square fit of Eq. (44) to the data (solid line). The observed decrease of C_{eff} is compatible with the logarithmic behavior of a dangerous irrelevant variable at the upper critical dimension. The reduced χ^2 of the fit is 0.16. L is in units of lattice constant.

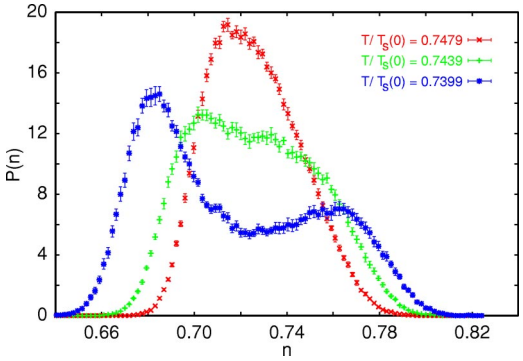

FIG. 11. Particle density distribution $P(n)$ (dimensionless) for three temperatures along a straight path given by Eq. (38) in the tricritical region as proposed by Eq. (35). The temperatures chosen are $T/T_s(0)=0.7479$ ($\times$), $T/T_s(0)=0.7439$ (+), and $T/T_s(0)=0.7399$ (*). The parameters of Eq. (38) are $T_t/T_s(0)=0.7439$, $\Delta_t/J=3.438$, and $\Delta_t'=5.0J/T_s(0)$. P and n are dimensionless.

for the effective coupling parameter, where $l_0=6.2$ is taken from Fig. 9 and c_0 and c_1 serve as fit parameters to the data. The solid line in Fig. 10 displays this fit with $c_0=9.9\pm0.2$ and $c_1=1.6\pm0.1$ and demonstrates that the expected behavior according to Eq. (44) is consistent with the data.

The degree of agreement between the finite-size scaling behavior observed and expected may also be considered as an *a posteriori* confirmation that the sequence of the pseudotricritical points gives a reasonable estimate for the location of the tricritical point. However, some confirmation from a different source would still be desirable.

D. Other distribution functions and the cumulant method

In order to locate the first-order coexistence line one may inspect the distribution function $P(n)$ of the particle density

$$n \equiv L^{-3} \sum_i t_i . \tag{45}$$

Near a first-order demixing transition $P(n)$ displays two peaks, one at a higher density corresponding to the spin (^{4}He) rich liquid and one at a lower density corresponding to the vacancy (^{3}He) rich liquid. At the tricritical point the two peaks coalesce and they separate increasingly as one follows the two-phase coexistence line towards lower temperatures. As a criterion to locate the coexistence line one may demand that the ratio of the statistical weights of the two liquids, i.e., the ratio of the areas under the respective peaks of $P(n)$, should not depend on temperature. However, this criterion is only approximate, because *a priori* it is not clear what the value of the weight ratio should be. An accurate criterion can be obtained from the evaluation of the field mixing [33] [see Eq. (37)]. From thermodynamic considerations one may determine a linear combination of particle and energy density such that the corresponding distribution function is symmetric on the coexistence line [33]. The generally unknown value of the weight ratio then has to be unity at coexistence. In principle, one may determine the correct mixing ratio of the densities from Eqs. (36) and (37). However, the statistical uncertainties of the coefficients given by Eq. (36) are too large for this purpose and their accurate evaluation is beyond the scope of this work.

For the vector BEG model the task of locating the first-order coexistence line is aided by the observation that the spin rich fluid displays long-ranged XY type (superfluid) order when the demixing transition occurs. Apart from the particle density distribution [see Eq. (45)] we therefore also observe the distribution function of the magnetic energy density ε_m defined by

$$\varepsilon_m \equiv -JL^{-3} \sum_{\langle ij \rangle} t_i t_j \cos(\theta_i - \theta_j). \tag{46}$$

For our choice $J=K$ the demixing transition will also be indicated by a double peak structure of the distribution function $P(\varepsilon_m)$. Note that this will no longer be the case for sufficiently large $K>J$, for which the demixing transition precedes the onset of long-ranged magnetic order. By monitoring both distribution functions along various paths in the (T,Δ) plane of the phase diagram and by applying the constant weight ratio criterion to both we have redetermined the slope of the coexistence line in the vicinity of (T_t,Δ_t) [see Eq. (35)] and found

$$\Delta_t' = (5.0 \pm 0.1) J/T_s(0). \tag{47}$$

Note that the new estimate given by Eq. (47) is consistent with the previous one given by Eq. (39). We furthermore observe that the two peaks indeed merge into a single but broader one very close to the estimate of (T_t,Δ_t) given by Eq. (35). We illustrate this for $P(n)$ in Fig. 11 for $L=36$ along a straight path in the phase diagram according to Eq. (38) for the choice $T_t/Ts(0)=0.7439$, $\Delta_t/J=3.438$, and $\Delta_t'=5.0J/T_s(0)$ [see Eq. (47)] for three temperatures. In order to obtain a clear double peak structure in $P(n)$ including the transition from and to a single peak along the chosen path, a substantial amount of finetuning for both T_t and Δ_t is required even for moderate system sizes. It is therefore very comforting that the values for T_t and Δ_t required to obtain

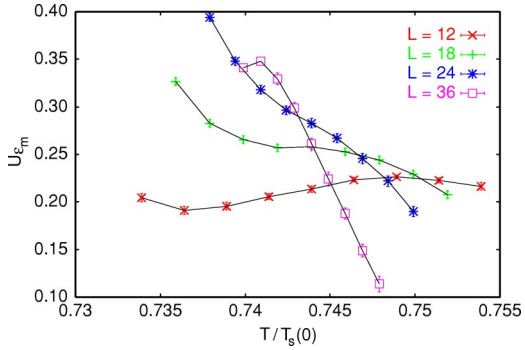

FIG. 12. Cumulant ratio U_{ε_m} (dimensionless) according to Eq. (48) as a function of temperature along the straight path used in Fig. 11 for $L=12$ (×), $L=18$ (+), $L=24$ (*), and $L=36$ (□). Pairs of symbols are connected linearly to guide the eye. A unique crossing cannot be identified (see main text).

Fig. 11 are already within the error bars of the extrapolation estimate of the tricritical point given by Eq. (35). The structure of $P(\varepsilon_m)$ essentially looks the same so we do not reproduce it here.

The location of the tricritical point along the coexistence line can be identified by a cumulant crossing of a suitably chosen density [33]. As we have not evaluated the field mixing here we use the cumulants of the magnetic energy density defined by Eq. (46) in order to investigate the cumulant crossing along the straight path used in Fig. 11. We define the Binder cumulant ratio for ε_m by

$$U_{\varepsilon_m} \equiv 1 - \frac{\langle (\varepsilon_m - \langle \varepsilon_m \rangle)^4 \rangle}{3 \langle (\varepsilon_m - \langle \varepsilon_m \rangle)^2 \rangle^2}. \tag{48}$$

The cumulant U_{ε_m} as a function of temperature for different system sizes is shown in Fig. 12. A unique crossing cannot be identified. However, the various crossings occur roughly where they are expected according to Eq. (35). If the smallest system $L=12$ is excluded, the crossings are located in the temperature interval $0.743 < T/T_s(0) < 0.747$ which includes the estimate given by Eq. (35) near the lower bound. The crossings for larger systems tend to occur at lower temperatures. One of the reasons that a unique crossing does not occur is that both ε_m and n contain corrections to the order parameter of the demixing transition which can only be eliminated by a properly chosen linear combination of these quantities [33]. A second reason is insufficient fine tuning for larger systems, which becomes visible in the nonmonotonic behavior of U_{ε_m} for $L=36$ at lower temperatures which leads to a second intersection with U_{ε_m} for $L=24$. Despite the quantitative shortcomings of Fig. 12, the investigation of the cumulant crossing in combination with the other evidence presented above provides some independent confirmation that our initial assertion about the shape of the tricritical order parameter distribution function according to Eq. (31) is correct within the accuracy needed for the purpose of this work.

Considerations in the spirit of Landau mean-field theory have played a major role in the analysis of our numerical data in the tricritical region. We therefore now turn to a detailed derivation of the Ginzburg-Landau model in the tricritical region of the vector BEG model.

VI. LANDAU-GINZBURG MODEL FOR ^{3}He-^{4}He MIXTURES

In this section we derive a two-parameter LG model describing bulk ^{3}He-^{4}He mixtures near tricriticality. This derivation follows the construction of the ϕ^4 model for the standard critical phenomena from the Ising model.

A. Derivation of the model

Our starting point is the modified VBEG model for which instead of continuum orientations of the spin vector $\mathbf{S}_i = (\cos\theta_i, \sin\theta_i)$ we consider L discrete orientations $\theta_i^{(l)} = 2\pi l/L$, $l=1,\ldots,L$, uniformly distributed over the unit circle with $L\to\infty$. With each orientation $\mathbf{S}_i^{(l)} = (\cos\theta_i^{(l)}, \sin\theta_i^{(l)})$ at the site i we associate the density $t_{i,l}$ with discrete values 0 or 1. The total density of ^{4}He at the site i is

$$t_i = \sum_{l=1}^{L} t_{i,l}. \tag{49}$$

As in the VBEG model, we consider the close-packing case in which a ^{3}He atom at site i corresponds to $t_i=0$ and a ^{4}He atom to $t_i=1$. Thus a lattice site i is either occupied by a ^{3}He atom ($t_i=0$) or a ^{4}He atom associated with one of the L orientations ($t_{i,l}=1$ for $l=l_0, t_{i,l}=0$ otherwise, so that $t_i = \sum_{l=1}^{L} t_{i,l} = 1$). The Hamiltonian of this effectively $(L+1)$-component mixture has the form

$$\mathcal{H} = -\sum_{\langle ij \rangle} \left\{ J \sum_{l=1}^{L} \sum_{l'=1}^{L} t_{i,l} t_{j,l'} \mathbf{S}_i^{(l)} \cdot \mathbf{S}_j^{(l')} + K t_i t_j \right\} + \Delta \sum_i t_i, \tag{50}$$

where $\mathbf{S}_i^{(l)} \cdot \mathbf{S}_j^{(l')} = \cos(\theta_i^{(l)} - \theta_j^{(l')})$.

In the Landau-Ginzburg model the effective Hamiltonian, depending on the local order-parameter fields, is obtained as a result of coarse-graining procedures. The procedure which gives an exact functional representation for the partition function for the corresponding microscopic Hamiltonian is the Hubbard-Stratonovitch transformation. The application of this method, however, is limited to microscopic Hamiltonians that can be expressed as a quadratic form. Here we use another approach [36].

Within the standard mean-field treatment of the lattice gas mixture defined by the Hamiltonian in Eq. (50), the ensemble-averaged occupancy $\rho_{i,l} = \langle t_{i,l} \rangle$ of the site i is obtained by minimizing the grand canonical function

$$\Omega^{MF}(\rho_{i,l}) = \mathcal{H}(\rho_{i,l}) + \sum_i f_{id}(\rho_{i,l}) \tag{51}$$

at fixed T and Δ. The resulting minimum of Ω^{MF} equals the equilibrium grand potential Ω_0. The ideal or noninteracting free-energy density for a $(L+1)$ component mixture on the close-packed lattice is [19]

$$f_{id}(\rho_{i,l}) = k_B T\left\{ (1-\rho_i)\ln(1-\rho_i) + \sum_{l=1}^{L} \rho_{i,l} \ln \rho_{i,l} \right\} \tag{52}$$

with $\rho_i = \Sigma_{l=1}^{L} \rho_{i,l}$.

In the following we shall treat ρ_i and $\rho_{i,l}$ as coarse-grained order parameter fields and adopt the mean-field grand canonical function Ω^{MF} form for the free energy of a particular local configuration of the order parameter. In the spatially uniform and orientationally disordered phase the equilibrium values of $\rho_{i,l}$ are constant and denoted by $\langle \rho_{i,l} \rangle = Q/L$ so that $\langle \rho_i \rangle = Q$. The actual values fluctuate around these mean values:

$$\rho_i = Q + \phi_i , \tag{53}$$

$$\rho_{i,l} = \frac{Q}{L} + \frac{\phi_i}{L} + \Delta\rho_{i,l} = \frac{\rho_i}{L} + \Delta\rho_{i,l} , \tag{54}$$

which implies $\langle \phi_i \rangle = 0$ and $\Sigma_l \Delta\rho_{i,l} = 0$ even without taking the thermal average. The fluctuation of the density $\rho_{i,l}$ at the site i consists of an orientationally uniform part ϕ_i/L related to the fluctuation ϕ_i of the total ^{4}He density, which is the same for all orientations, and a contribution $\Delta\rho_{i,l}$ as an excess density of ^{4}He in the orientation $\mathbf{S}_i^{(l)}$.

Assuming $\Delta\rho_{i,l}$ and ϕ_i to be small we expand $\Omega^{MF}(\rho_i, \rho_{i,l})$ in power series of the fluctuation fields $\Delta\rho_{i,l}$ and ϕ_i about the equilibrium value $\Omega_0^{MF}(\rho_i = Q, \rho_{i,l} = Q/L)$. Since we aim for deriving an effective Hamiltonian describing bulk ^{3}He-^{4}He mixtures near tricriticality, in the expansion we keep terms to the sixth order in $\Delta\rho_{i,l}$ and to quadratic order in ϕ_i. A standard Taylor expansion gives

$$\Omega^{MF}(\rho_i, \rho_{i,l}) - \Omega_0^{MF}(Q, Q/L) = \sum_{j=2}^{6} \Omega_j^{MF}(\phi_i, \Delta\rho_{i,l}) . \tag{55}$$

The contribution linear in the fluctuation fields Ω_1^{MF} vanishes since we expand Ω^{MF} around its minimum. The other terms are

$$\Omega_2^{MF}(\phi_i, \Delta\rho_{i,l}) = -\sum_{\langle i,j \rangle} \left\{ K\phi_i\phi_j + J\sum_{l=1}^{L}\sum_{l'=1}^{L} \Delta\rho_{i,l}\Delta\rho_{j,l'} \mathbf{S}_i^{(l)} \cdot \mathbf{S}_j^{(l')} \right\} + \frac{k_B T}{2} \sum_i \left\{ \frac{1}{Q(1-Q)} \phi_i^2 + \sum_{l=1}^{L} \frac{L}{Q} (\Delta\rho_{i,l})^2 \right\}, \tag{56}$$

$$\Omega_3^{MF}(\phi_i, \Delta\rho_{i,l}) = -\frac{k_B T}{2} \sum_i \sum_{l=1}^{L} \left\{ \frac{L}{Q^2} \phi_i (\Delta\rho_{i,l})^2 + \frac{1}{3} \frac{L^2}{Q^2} (\Delta\rho_{i,l})^3 \right\}, \tag{57}$$

$$\Omega_4^{MF}(\phi_i, \Delta\rho_{i,l}) = \frac{k_B T}{2} \sum_i \sum_{l=1}^{L} \left\{ \frac{2}{3} \frac{L^2}{Q^3} \phi_i (\Delta\rho_{i,l})^3 + \frac{L}{Q^3} \phi_i^2 (\Delta\rho_{i,l})^2 + \frac{1}{6} \frac{L^3}{Q^3} (\Delta\rho_{i,l})^4 \right\}, \tag{58}$$

$$\Omega_5^{MF}(\phi_i, \Delta\rho_{i,l}) = -\frac{k_B T}{2} \sum_i \sum_{l=1}^{L} \left\{ \frac{1}{2} \frac{L^3}{Q^4} \phi_i (\Delta\rho_{i,l})^4 + \frac{L^2}{Q^4} \phi_i^2 (\Delta\rho_{i,l})^3 + \frac{1}{10} \frac{L^4}{Q^4} (\Delta\rho_{i,l})^5 \right\}, \tag{59}$$

$$\Omega_6^{MF}(\phi_i, \Delta\rho_{i,l}) = \frac{k_B T}{2} \sum_i \sum_{l=1}^{L} \left\{ \frac{2}{5} \frac{L^4}{Q^5} \phi_i (\Delta\rho_{i,l})^5 + \frac{L^3}{Q^5} \phi_i^2 (\Delta\rho_{i,l})^4 + \frac{1}{15} \frac{L^5}{Q^5} (\Delta\rho_{i,l})^6 \right\}. \tag{60}$$

The excess density in the orientation $\mathbf{S}_i^{(l)}$ is a periodic function of l with period L. Therefore, it can be expanded into a discrete Fourier series

$$\Delta\rho_{i,l} = \frac{Q}{2L} \sum_{k=1}^{L-1} u_{i,k} e^{i(2\pi/L)kl} , \tag{61}$$

where we have chosen $(Q/2L)$ as a normalization constant. The term corresponding to $k=0$ is excluded from the expansion due to the constraint $\Sigma_{l=1}^{L} \Delta\rho_{i,l} = 0$. Since $\Delta\rho_{i,l}$ is a real function, the Fourier components $u_{i,k}$ and $u_{i,L-k}$ are related by $u_{i,k}^* = u_{i,L-k}$. Now, we neglect higher modes in the Fourier expansion (61) and approximate the excess density in the orientation $\mathbf{S}_i^{(l)}$ by

$$\Delta\rho_{i,l} \approx \frac{Q}{2L} (u_{i,1} e^{i(2\pi/L)l} + u_{i,L-1} e^{-i(2\pi/L)l}) . \tag{62}$$

Using $u_{i,k}^* = u_{i,L-k}$ and expressing $u_{i,1}$ in terms of its amplitude $|u_i|$ and a phase ζ_i we write Eq. (62) as

$$\Delta\rho_{i,l} \approx \frac{Q}{2L} |u_i| (e^{i((2\pi/L)l + \zeta_i} + e^{-i((2\pi/L)l + \xi_i)}) = \frac{Q}{L} |u_i| \cos[(2\pi/L)l + \zeta_i] = \frac{Q}{L} \mathbf{S}_i^{(l)} \cdot \mathbf{u}_i , \tag{63}$$

where $\mathbf{u}_i \equiv |u_i| \exp(i\zeta_i)$.

The approximation (63) is a ''coarse-graining'' procedure which reduces degrees of freedom. The $L-1$ independent quantities describing the orientational degrees of freedom are replaced by a two-component vector field $\mathbf{u}_i$.

We define the effective Hamiltonian for the order parameter fields ϕ and $\mathbf{u}$ as

$$\Omega^{eff}(\phi_i, \mathbf{u}_i) \equiv \Omega^{MF}(\rho_i, \rho_{i,l}) - \Omega_0^{MF}(Q, Q/L). \tag{64}$$

Using Eq. (63) in Eqs. (56–60) we obtain

$$\Omega^{eff} = \Omega_2^{eff} + \Omega_{int}^{eff} \tag{65}$$

with

$$\begin{aligned}\Omega_2^{eff}(\phi_i, \mathbf{u}_i) = -\sum_{\langle i,j \rangle} \Bigg\{ & K\phi_i\phi_j + \frac{Q^2}{L^2} J \sum_{l=1}^{L} \sum_{l'=1}^{L} (\mathbf{S}_i^{(l)} \cdot \mathbf{u}_i) \\ & \times (\mathbf{S}_j^{(l')} \cdot \mathbf{u}_j) \mathbf{S}_i^{(l)} \cdot \mathbf{S}_j^{(l')} \Bigg\} \\ & + \frac{k_B T}{2} \sum_i \Bigg\{ \frac{1}{Q(1-Q)} \phi_i^2 \\ & + \frac{Q}{L} \sum_{l=1}^{L} (\mathbf{S}_i^{(l)} \cdot \mathbf{u}_i)^2 \Bigg\},\end{aligned} \tag{66}$$

$$\begin{aligned}\Omega_{int}^{eff} = \frac{k_B T}{2} \sum_i \Bigg\{ & -\phi_i \frac{1}{L} \sum_{l=1}^{L} (\mathbf{S}_i^{(l)} \cdot \mathbf{u}_i)^2 \\ & + \phi_i^2 \frac{1}{QL} \sum_{l=1}^{L} (\mathbf{S}_i^{(l)} \cdot \mathbf{u}_i)^2 + \frac{1}{6} \frac{Q}{L} \sum_{l=1}^{L} (\mathbf{S}_i^{(l)} \cdot \mathbf{u}_i)^4 \\ & - \frac{1}{2} \phi_i \frac{1}{L} \sum_{l=1}^{L} (\mathbf{S}_i^{(l)} \cdot \mathbf{u}_i)^4 + \phi_i^2 \frac{1}{QL} \sum_{l=1}^{L} (\mathbf{S}_i^{(l)} \cdot \mathbf{u}_i)^4 \\ & + \frac{1}{15} \frac{Q}{L} \sum_{l=1}^{L} (\mathbf{S}_i^{(l)} \cdot \mathbf{u}_i)^6 \Bigg\}.\end{aligned} \tag{67}$$

We note that in the above expression terms containing sums over all orientations of odd powers of $(\mathbf{S}_i^{(l)} \cdot \mathbf{u}_i)$ vanish.

As the next step we take the limit $L \to \infty$. This amounts to replacing $(1/L)\Sigma_{l=1}^{L}$ by $(1/2\pi)\int_0^{(2\pi)} d\theta$ and leads to the following relations $[\mathbf{S}_i^{(l)} = (\cos\theta_i^{(l)}, \sin\theta_i^{(l)})]$:

$$\frac{Q}{L} \sum_{l=1}^{L} (\mathbf{S}_i^{(l)} \cdot \mathbf{u}_i)^2 \to \frac{Q}{2\pi} \int_0^{2\pi} d\theta_i^{(l)} (\mathbf{S}_i^{(l)} \cdot \mathbf{u}_i)^2 = \frac{Q}{2} |\mathbf{u}_i|^2, \tag{68}$$

$$\frac{Q}{L} \sum_{l=1}^{L} (\mathbf{S}_i^{(l)} \cdot \mathbf{u}_i)^4 \to \frac{Q}{2\pi} \int_0^{2\pi} d\theta_i^{(l)} (\mathbf{S}_i^{(l)} \cdot \mathbf{u}_i)^4 = \frac{3Q}{8} |\mathbf{u}_i|^4, \tag{69}$$

$$\frac{Q}{L} \sum_{l=1}^{L} (\mathbf{S}_i^{(l)} \cdot \mathbf{u}_i)^6 \to \frac{Q}{2\pi} \int_0^{2\pi} d\theta_i^{(l)} (\mathbf{S}_i^{(l)} \cdot \mathbf{u}_i)^6 = \frac{5Q}{16} |\mathbf{u}_i|^6, \tag{70}$$

and

$$\begin{aligned}\frac{Q^2}{L^2} \sum_{l=1}^{L} \sum_{l'=1}^{L} & (\mathbf{S}_i^{(l)} \cdot \mathbf{u}_i)(\mathbf{S}_j^{(l')} \cdot \mathbf{u}_j) \mathbf{S}_i^{(l)} \cdot \mathbf{S}_j^{(l')} \\ & \to \frac{Q^2}{4\pi^2} \int_0^{2\pi} d\theta_i^{(l)} \int_0^{2\pi} d\theta_j^{(l')} (\mathbf{S}_i^{(l)} \cdot \mathbf{u}_i)(\mathbf{S}_j^{(l')} \cdot \mathbf{u}_j) \mathbf{S}_i^{(l)} \cdot \mathbf{S}_j^{(l')} \\ & = \frac{Q^2}{4} \mathbf{u}_i \cdot \mathbf{u}_j.\end{aligned} \tag{71}$$

Finally, we assume that the fluctuating fields ϕ_i and $\mathbf{u}_i$ vary slowly on the length scale of the lattice constant a. The continuum limit is obtained by considering $a \to 0$, considering i as a continuous variable $\mathbf{r}$, and ϕ_i and $\mathbf{u}_i$ turning into $\phi(\mathbf{r})$ and $\mathbf{u}(\mathbf{r})$, respectively, while keeping the total volume $V = a^3 N$ fixed. In this limit, one has

$$\sum_i \to a^{-3} \int d\mathbf{r}. \tag{72}$$

For f being the smooth continuation to continuous arguments of a function defined on a lattice we use the following approximations $(a \to 0)$:

$$\sum_{k=1}^{d} f(\mathbf{r} + a\mathbf{e}_k) \to d f(\mathbf{r}) + a \sum_{k=1}^{d} \frac{\partial f}{\partial r_k} + \frac{a^2}{2} \sum_{k=1}^{d} \frac{\partial^2 f}{\partial r_k^2} + \cdots \tag{73}$$

and

$$\sum_{k=1}^{d} \{f(\mathbf{r} + a\mathbf{e}_k) + f(\mathbf{r} - a\mathbf{e}_k)\} \to 2d f(\mathbf{r}) + a^2 \sum_{k=1}^{d} \frac{\partial^2 f}{\partial r_k^2} + \cdots, \tag{74}$$

where $\mathbf{e}_k, k = 1, \ldots, d$ are the unit lattice vectors. Thus

$$\begin{aligned}\sum_{\langle i,j \rangle} f_i f_j & \to \frac{1}{2} a^{-3} \int d^3\mathbf{r} \sum_{k=1}^{d} f(\mathbf{r}) \{f(\mathbf{r} + a\mathbf{e}_k) + f(\mathbf{r} - a\mathbf{e}_k)\} \\ & \to \frac{1}{2} a^{-3} \int d^3 r \{2d f^2(\mathbf{r}) - a^2 (\nabla f)^2\}.\end{aligned} \tag{75}$$

As a result Eq. (64) is replaced by

$$\Omega^{eff} = K[\Omega_G + \Omega_{int}] \tag{76}$$

with the Gaussian contribution Ω_G, in which the fields ϕ and $\mathbf{u}$ are uncoupled,

$$\Omega_G = \int d\mathbf{r} \left\{ \frac{1}{2} a_1 \phi^2 + \frac{1}{2} (\nabla\phi)^2 + \frac{1}{2} a_2 |\mathbf{u}|^2 + \frac{1}{2} c (\nabla \mathbf{u})^2 \right\}, \tag{77}$$

and the interaction contribution, which couples ϕ and $\mathbf{u}$,

$$\Omega_{int}=\int d\mathbf{r}\{r_1\phi|\mathbf{u}|^2+a_{12}\phi^2|\mathbf{u}|^2+b|\mathbf{u}|^4+r_2\phi|\mathbf{u}|^4 + b_{12}\phi^2|\mathbf{u}|^4+e|\mathbf{u}|^6\}, \tag{78}$$

where we have chosen the length unit such that $a=1$.

The coupling constants in the effective functional are given explicitly by

$$a_1=\frac{k_BT}{K}\frac{1}{Q(1-Q)}-z, \tag{79}$$

$$a_2=\frac{k_BT}{K}\frac{Q}{2}-\frac{zQ^2}{4}\frac{J}{K}, \tag{80}$$

$$c=\frac{Q^2}{4}\frac{J}{K}, \tag{81}$$

$$r_1=-\frac{1}{4}\frac{k_BT}{K}, \quad r_2=-\frac{3}{32}\frac{k_BT}{K}, \tag{82}$$

$$b=\frac{Q}{32}\frac{k_BT}{K}, \quad e=\frac{Q}{96}\frac{k_BT}{K}, \tag{83}$$

$$a_{12}=\frac{1}{4Q}\frac{k_BT}{K}, \quad b_{12}=\frac{3}{16Q}\frac{k_BT}{K}. \tag{84}$$

Equations (77), (78), and (79)–(84) define the Landau-Ginzburg model for ^{3}He-^{4}He mixtures in terms of thermodynamical quantities and two parameters, J and K, characterizing the system.

B. λ line and tricritical point

In this subsection we determine the λ line and a tricritical point within mean-field theory for the LG model derived in the preceding subsection. To this end we consider spatially uniform order parameter fields.

Mean-field theory amounts to approximating the thermodynamic free energy by the minimum of the effective Hamiltonian which corresponds to the saddle point path contribution to the partition function,

$$\beta F_{MF}=\min_{\phi,\mathbf{u}}\beta\Omega^{eff}[\phi,\mathbf{u}]. \tag{85}$$

The mean-field solution for $\phi(\mathbf{r})$ is determined by

$$\frac{\delta\Omega^{eff}}{\delta\phi(\mathbf{r})}=0. \tag{86}$$

For spatially uniform fields the above minimum condition yields the following relation between ϕ and $|\mathbf{u}|$:

$$\phi(a_1+2a_{12}|\mathbf{u}|^2+2b_{12}|\mathbf{u}|^4)+r_1|\mathbf{u}|^2+r_2|\mathbf{u}|^4=0. \tag{87}$$

Near a tricritical point both the fields ϕ and $|\mathbf{u}|$ are small. Therefore it is sufficient to consider only a linear coupling between $|\mathbf{u}|^2$ and ϕ, neglecting the higher-order terms,

$$\phi=-\frac{r_1}{a_1}|\mathbf{u}|^2+2\frac{r_1a_{12}}{a_1^2}|\mathbf{u}|^4+O(|\mathbf{u}|^6). \tag{88}$$

Inserting Eq. (88) into Eqs. (77) and (78) we obtain

$$\frac{\Omega^{eff}}{V}=\frac{1}{2}a_2|\mathbf{u}|^2+\left(b-\frac{1}{2}\frac{r_1^2}{a_1}\right)|\mathbf{u}|^4+e'|\mathbf{u}|^6 \tag{89}$$

with

$$e'=a_{12}\frac{r_1^2}{a_1^2}-\frac{r_1r_2}{a_1}+e. \tag{90}$$

The condition $a_2=0$ yields the equation for the critical line which is in agreement with Eq. (21). If a_1 is negative, e' is positive and there is a tricritical point determined by

$$a_2=0, \quad b-\frac{1}{2}\frac{r_1^2}{a_1}=0. \tag{91}$$

The solution of these two equations coincides with the expressions given by Eqs. (23) and (24), i.e., the tricritical point of this LG model is located at the same temperature and concentration of ^{3}He atoms as the tricritical point in the VBEG model studied in Sec. III within mean-field approximation.

VII. SUMMARY AND DISCUSSION

By using molecular-field approximations and Monte Carlo simulations we have investigated a three-dimensional version of the generalized spin-1 Blume-Emery-Griffith model [Eq. (1)] of ^{3}He-^{4}He mixtures with a two-component vector order parameter, mimicking the phase of the wave function of ^{4}He atoms. This work is a first step to study the Casimir force and other surface and finite-size effects in ^{3}He-^{4}He mixture films near their tricritical point. We have obtained the following main results.

(1) The topology of the phase diagram depends on the ratio of the interaction parameters K/J, where K is related to the $^{\alpha}$He-$^{\beta}$He interactions [Eq. (2)] and J to the superfluid density [Eq. (4)]. There are three different types of the phase diagram, which are similar to those found in the BEG model within the molecular-field approximation. For large values of K/J, i.e., for $K/J>2.016\,81$, there exist three different phases: a ^{3}He-rich normal fluid, a ^{4}He-rich normal fluid, and a ^{4}He-rich superfluid (see Fig. 1). As the temperature is lowered, the mixed normal fluid phase separates into two normal fluids differing by the concentration x of ^{3}He. This phase separation ends at a critical point. At lower temperature, the phase separation is into a superfluid and a normal fluid. The λ line $T_s(x)$ of second-order phase transitions between a ^{4}He-rich normal fluid and a ^{4}He-rich superfluid terminates at the ^{4}He-rich branch of the phase-separation curve at the critical end point. This ''critical end-point'' type of the phase diagram was the only one found in previous studies [15,16] of the two-dimensional version of the model. In three dimensions we find two additional topologies of the phase diagram

as the ratio K/J is decreased. For $1.4298 < K/J < 2.016\,81$ the phase diagram is the richest (see Fig. 2). As in the previous case, there are three different phases and a critical point of the phase-separation curve between two normal fluids differing by the concentration of ^{3}He. In addition, there is a tricritical point at the end of the λ line beyond which a first-order phase transition between a ^{4}He-rich superfluid and a ^{4}He-rich normal fluid takes place. There is also a triple point at which three different phases coexist at different concentrations. For $K/J < 1.4298$ the phase diagram simplifies (see Fig. 3). There is no longer a ^{4}He-rich normal fluid phase and a critical point. The λ line meets the first-order phase-separation line between ^{4}He-rich superfluid and a ^{3}He-rich normal fluid at the tricritical point. The λ line is given by $T_s(x) = zJ(1-x)/2$, where z is the coordination number of the lattice. The temperature of the tricritical point is $T_A/T_s(0) = (1+2K/J)/(2+2K/J)$ [Eq. (23)] and the concentration x_A of ^{3}He at this point is given by $T_A/T_s(0) = 1 - x_A$ [Eq. (24)]. This type of the phase diagram is, except at the very low temperatures when the Fermi statistic of ^{3}He plays the dominant role, similar to that observed experimentally, although in our model x_A is always smaller than 0.5 whereas $x_A^{exp} = 0.669$. For a given topology of a phase diagram changing parameters of a model does not affect our main results.

(2) The existence of the tricritical point is confirmed by Monte Carlo simulations and in the units $[T_t/T_s(0), \Delta_t/J]$ it coincides with the mean-field prediction remarkably well (see Fig. 3). At the tricritical point the order parameter distribution function takes its mean-field form, where the presence of logarithmic corrections could not be excluded within the accuracy of the existing data. On the other, hand finite-size scaling of several thermodynamic quantities reveals the presence of logarithmic corrections in accordance with theoretical expectations. The two-phase coexistence line in the (T, Δ) plane of the phase diagram has been determined from a constant weight ratio criterion for energy and density histograms. The location of the tricritical point is also indicated by a crossing of the cumulant ratio of the magnetic portion of the energy density measured along the coexistence line (see Fig. 12). We conclude that mean-field theory provides a reliable approach for studying the VBEG model in $d = 3$.

(3) Starting from the VBEG model and discretizing the orientations of the spin vector we have derived the continuum Landau-Ginzburg model for ^{3}He-^{4}He mixtures near the tricritical point encompassing the concentration field ϕ and a two-component vector field $\mathbf{u}$ corresponding to the orientational order. In the effective Hamiltonian we consider the modulus of $\mathbf{u}$ up to its sixth power and the field ϕ up to quadratic terms, which is sufficient to study a tricritical point. The coupling constants appearing in this Landau-Ginzburg theory are given explicitly in terms of thermodynamical quantities, the temperature, the mean concentration of ^{4}He, and the two interaction parameters J and K characterizing the VBEG model. Mean-field theory for this LG model yields the same equation for the critical λ line as the molecular-field approximation for the lattice VBEG model. The LG model provides a linear coupling between $|\mathbf{u}|^2$ and ϕ which yields the same coordinates of the tricritical point as the lattice VBEG model.

ACKNOWLEDGMENTS

A.M. is grateful for the hospitality accorded by the Max-Planck-Institut für Metallforschung in Stuttgart, Germany. She appreciates fruitful discussions with Alina Ciach. This work was partially funded by KBN Grant No. 4 T09A 066 22.

[1] M. Krech, *The Casimir Effect in Critical Systems* (World Scientific, Singapore, 1994), and references therein; M. Krech J. Phys.: Condens. Matter **11**, R391 (1999).
[2] R. Garcia and M.H.W. Chan, Phys. Rev. Lett. **83**, 1187 (1999).
[3] M. Krech and S. Dietrich, Phys. Rev. Lett. **66**, 345 (1991); **67**, 1055 (1991).
[4] M. Krech and S. Dietrich, Phys. Rev. A **46**, 1886 (1992).
[5] M. Krech and S. Dietrich, Phys. Rev. A **46**, 1922 (1992).
[6] A. Mukhopadhyay and Bruce M. Law, Phys. Rev. Lett. **83**, 772 (1999); a quantitative understanding of these experimental data has not yet been reached.
[7] R. Garcia and M.H.W. Chan, Phys. Rev. Lett. **88**, 086101 (2002).
[8] T. Ueno, S. Balibar, T. Mizusaki, F. Caupin, and E. Rolley, Phys. Rev. Lett. **90**, 116102 (2003); T. Ueno, S. Balibar, T. Mizusaki, F. Caupin, M. Fechner, and E. Rolley, J. Low Temp. Phys. **130**, 543 (2003).
[9] J.-P. Laheurte, J.-P. Romagnan, and W.F. Saam, Phys. Rev. B **15**, 4214 (1977).
[10] S. Leibler and L. Peliti, Phys. Rev. B **29**, 1253 (1984); L. Peliti and S. Leibler, J. Phys. Lett. (France) **45**, L591 (1984).
[11] D. McQueeney, G. Agnolet, and J.D. Reppy, Phys. Rev. Lett. **52**, 1325 (1984).
[12] J.M. Kosterlitz and D.J. Thouless, J. Phys. C **5**, L124 (1972).
[13] S. Dietrich, in *Phase Transitions and Critical Phenomena*, edited by C. Domb and J. L. Lebowitz (Academic, London, 1988), Vol. 12, p. 1.
[14] G. Ahlers and D.S. Greywall, Phys. Rev. Lett. **29**, 849 (1972); H.A. Kierstead, J. Low Temp. Phys. **35**, 25 (1979); E.H. Graf, D.M. Lee, and J.D. Reppy, Phys. Rev. Lett. **19**, 417 (1967).
[15] J.L. Cardy and D.J. Scalpino, Phys. Rev. B **19**, 1428 (1979).
[16] A.N. Berker and D.R. Nelson, Phys. Rev. B **19**, 2488 (1979).
[17] M. Blume, V.J. Emery, and R.B. Griffiths, Phys. Rev. A **4**, 1071 (1971).
[18] G. Baym and C. Pethick, *Landau Fermi-Liquid Theory* (Wiley, New York, 1991).
[19] See, for example, G. M. Bell and D. A. Lavis, *Statistical Mechanics of Lattice Models* (Ellis Horwood, Chichester, 1989).
[20] D.J. Bishop and J.D. Reppy, Phys. Rev. Lett. **40**, 1727 (1978).
[21] N.D. Mermin and H. Wagner, Phys. Rev. Lett. **17**, 1133 (1966).
[22] See, for example, P. M. Chaikin and T. C. Lubensky, *Principles of Condensed Matter Physics* (Cambridge University

Press, Cambridge, England, 1995).

[23] In the other approach to determine variational minima to Eq. (7) a parametrization of ρ_i in terms of order parameters $\langle \phi_i \rangle$ (for example, Q, M_x, and M_y) can be chosen. This parametrization must satisfy the constraints $\mathrm{Tr}\rho_i = 1$ and $\mathrm{Tr}\rho_i \phi_i = \langle \phi_i \rangle$. The variational parameters are simply order parameters and F_{ρ_0} is the Helmholtz free energy functional $F(\langle \phi \rangle)$. This procedure is less general than the one used in the present paper.

[24] *Handbook of Mathematical Functions*, edited by M. Abramowitz and I. A. Stegun (Dover, New York, 1972).

[25] M.E. Fisher and M.C. Barbosa, Phys. Rev. B **43**, 11177 (1991).

[26] N. Metropolis, A.W. Rosenbluth, M.N. Rosenbluth, A.H. Teller, and E. Teller, J. Chem. Phys. **21**, 1087 (1953).

[27] U. Wolff, Phys. Rev. Lett. **62**, 361 (1989).

[28] K. Chen, A.M. Ferrenberg, and D.P. Landau, Phys. Rev. B **48**, 3249 (1993).

[29] J.A. Plascak, A.M. Ferrenberg, and D.P. Landau, Phys. Rev. E **65**, 066702 (2002).

[30] A.M. Ferrenberg, D.P. Landau, and Y.J. Wong, Phys. Rev. Lett. **69**, 3382 (1993); L.N. Shchur and H.W.J. Blöte, Phys. Rev. E **55**, R4905 (1997).

[31] T. Nagasima, Y. Sugita, A. Mitsutake, and Y. Okamoto, Comput. Phys. Commun. **146**, 69 (2002).

[32] A.M. Ferrenberg and R.H. Swendsen, Phys. Rev. Lett. **61**, 2635 (1988); **63**, 1195 (1989).

[33] N.B. Wilding and P. Nielaba, Phys. Rev. E **53**, 926 (1996).

[34] M. Krech (unpublished); see also W. Janke and H. Kleinert, Nucl. Phys. **B270**, 135 (1986)

[35] D. Lawrie and S. Sarbach, in *Phase Transitions and Critical Phenomena*, edited by C. Domb and J. L. Lebowitz (Academic, London, 1984), Vol. 9, p. 2.

[36] A. Ciach, J. Chem. Phys. **104**, 2376 (1996).